DOI: 10.61782/fa.2025.0424

FORUM ACUSTICUM EURONOISE 2025

GPU-BASED AEROACOUSTIC SIMULATION OF LOW-SPEED AXIAL FANS ACROSS THEIR CHARACTERISTIC FAN CURVES

Alessandra Verza[1*] **Peter Altmann**[2] **Lars Erbig**[2]
[1] Siemens Digital Industries Software, Spain
[2] Siemens Digital Industries Software, Germany

ABSTRACT

Over the past years, several papers dealt with numerical simulations of EAA's axial fan benchmark at its design point. Since all these publications used different simulation techniques and mesh types, but still delivered meaningful results, we assess how different levels of mesh resolution on the fan surfaces and motion modeling approaches impact the accuracy of the simulations when looking at more extreme operating conditions close to stall or free flow. Our simulations are based on constant-density Large Eddy Simulation coupled to a Perturbed Convective Wave equation and are run on 8 Nvidia A100 GPUs, which allows us to return results significantly more quickly than on CPUs. We find that accurately predicting aerodynamic quantities on all considered operating points requires a fine normal, and surface resolution on the fan blades as well as accurate motion modeling. In contrast, the acoustic far field predictions on all operating points except the free-flow condition are significantly less dependent on meshing and motion modeling decisions.

Keywords: *fan noise, large eddy simulation, les, pcwe, gpu.*

1. INTRODUCTION

Fast and reliable aeroacoustics simulation methods are key to enabling manufacturers to develop fan designs for a broad set of applications, such as automotive, wearable technology and appliances. Lowering the noise from components is one of the main concerns for fan manufacturers.

The most common approach in literature to this kind of problem mainly focuses on finding the best set up to accurately resolve the design operating point. This can be observed in numerous papers, for example by Ghodake et al. [1] and Antoniou et al. [2] show results on different meshes both at 1.4 m^3/s, and Erbig et al. [3] solved for the same mass flow rate on very coarse and fine grids. All these papers present good correlation with the experimental results, but so far there have been significantly less research efforts on the robustness of a simulation across a range of operating conditions.

The purpose of this study was to understand the variation in accuracy of the results when key aspects of the simulation and operating conditions were changed. In particular, changes in mesh resolution and motion modeling methods were studied to understand their effects on both aerodynamic and acoustic fields.

The experimental benchmark data that this study refers to, was based on a test series run by Krömer at the Friedrich-Alexander Universität Erlangen-Nürnberg on low-pressure axial fans [4].

Both aerodynamics and acoustic results are compared to the test data across the different mass flow rates to provide better insight into the requirements needed for the set up according to which quantities are of interest for the user.

2. THEORY

In this section, the theoretical background of the simulations is introduced, distinguishing between flow and acoustics modeling, and modeling of the fan motion itself. Finally, the evaluated quantities of interest are introduced.

[*] ***Corresponding author***: *alessandra.verza@siemens.com.*

2.1 Flow and Acoustic Modeling

The simulations follow a hybrid finite-volume approach that splits the aeroacoustic problem into a constant-density Large Eddy Simulation (LES) that is one-way coupled to a Perturbed Convective Wave Equation (PCWE) that uses instantaneous flow fields to model convective effects, as originally introduced by Piepiorka and von Estorff [5]. Both flow and acoustics use a 2nd order discretization in space and an implicit 2nd order temporal discretization. For flow, the temporal discretization is based on backward differencing, and the PCWE is discretized using a Newmark Alpha scheme [3]. It is worth noting that a constant density flow simulation allows fixing the volumetric flow rate at the inlet and is therefore particularly well suited to simulate a range of operating points across an unknown characteristic fan curve.

2.2 Motion Modeling

There are different approaches to model motion or to be more precise fan rotation in numerical simulations. The so-called moving reference (MRF) method was originally developed for axial flows and utilizes momentum equation source terms to approximate rotation [6]. Since no real rotation takes place, it is a numerically cost efficient, pragmatic approach, but with limitations in terms of accuracy. A high-fidelity simulation requires the real motion of the fan. This aspect is enabled with the so-called rigid body motion (RBM) model. The simulation domain gets divided into two parts/regions: the stationary region is the test chamber fluid volume, and the rotating region is the fluid volume surrounding the fan. The latter gets the fan rotation rate assigned and is normally modelled as a cylinder and contains the fan and in case of an axisymmetric shroud the entire shroud fluid volume. Consequently, the interface between the two regions must be re-calculated at every time-step. Past publications [3, 7] used intersection algorithms that lead to topologically valid cells, this paper is based on a more lightweight, "metrics-based", intersection algorithm that does not generate new polygonal faces [6]. While this approach is potentially less accurate, it also minimizes the memory footprint of the intersection and is better suited for running on GPUs.

2.3 Quantities of Interest

The aerodynamic performance of the fan is characterized by its total-to-static efficiency η_{ts} and its total-to-static pressure coefficient ψ_{ts}. Let Q denote the volume flow rate through the fan, and Δp_{ts} its total-to-static pressure difference. Then, the total-to-static pressure coefficient is defined by

$$\psi_{ts} = \frac{2\Delta p_{ts}}{\rho(\pi n d_{\text{fan}})^2} \quad , \tag{1}$$

where ρ is the fluid density, n is the number of blades, and d_{fan} the fan diameter. The total-to-static efficiency is given by

$$\eta_{ts} = \frac{Q\Delta p_{ts}}{M_s 2\pi n} \quad , \tag{2}$$

where M_s is the shaft torque. The acoustic performance of the fan is presented at far field microphones by evaluating its Sound Power Level (SWL) from the A-weighted time signals at the 7 microphones following the standard procedure outlined in DIN EN ISO 3746:2011-03.

3. TEST CASE

3.1 Experimental Setup

The original case was published by the European Acoustics Association [4] including both acoustics and aerodynamics experimental data. The fan was tested in a standardized inlet test chamber with a flow straightener upstream, and the exact volume flow rates were achieved by using an auxiliary fan in the inlet section. The acoustic experimental data was collected across 7 microphones located in an arc 1 m away from the inlet nozzle of the fan, as can be seen in Figure 1.

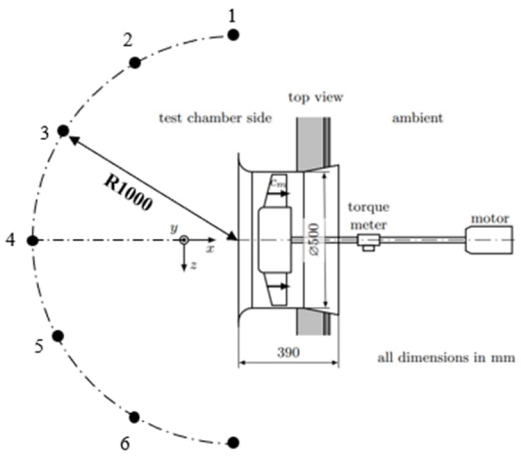

Figure 1. Detail of experimental setup with microphone arc [4].

The geometry here considered consists of an axial fan with a diameter of $d_{\text{fan}} = 0.495\,\text{m}$ and with $n = 9$ blades (referred to as "S1U" by Krömer [8]), mounted inside a duct 0.5 m in diameter, showed in Figure 2. The fan was tested across its complete operating curves, from stall to free flow, which means the inflow rate varied between 0.2 m^3/s to 2.1 m^3/s. Additional equipment was used to provide more

data on the flow behavior, such as time signals from differential pressure transducers to measure wall pressure fluctuations in the duct, and Laser Doppler Anemometer measurements on both sides of the fan.

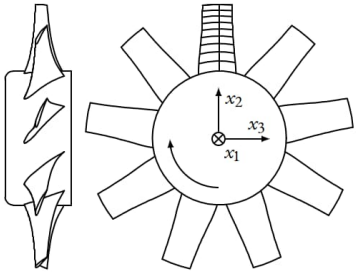

Figure 2. Tested axial fan with unskewed blades [4].

3.2 Numerical Setup

The computational setup replicates the experimental test facility and consists of two large rectangular chambers that are separated by a partition and the duct which hosts the axial fan. The top, bottom and side surfaces and the partition are modeled as non-reflecting, rigid walls. Inlet and outlet boundaries are parallel to the partition and prescribe a mass flow rate at the suction side and enforce a pressure on the pressure side of the fan (as shown in Figure 3). A hex dominated, so-called trimmed mesh in combination with prism layers at the surfaces was used to discretize the simulation domain. In total four different volume meshes were generated to analyze the impact of spatial discretization on runtimes and accuracy. The global mesh size (base size) for all meshes was 13.6 mm. Table 1 provides an overview of the relevant mesh parameters, relative to the base size if applicable, to create the different volume meshes. The total cell count varies between 55 M for the finest and 29 M for the coarsest mesh.

Table 1. Investigated volume meshes.

	Fan prism layers	Prism layer thickness (mm)	Fan target surface size (mm)	Fan minimum surface size (mm)	Volume cells (× 1E6)
Mesh 1	8	0.50	0.43	0.11	55
Mesh 2	2	0.75	0.43	0.11	40
Mesh 3	2	0.75	0.85	0.21	30
Mesh 4	2	0.75	1.70	0.43	26

A hemisphere was used to refine the mesh from the fan up to the far-field microphone locations. To capture the propagating sound waves, a uniform mesh size of 6.8 mm was used. This spatial resolution ensures 12 cells per wavelength up to 4 kHz.
The following image of Mesh 1, the finest volume mesh with around 55 M cells, visualizes the simulation domain, the overall mesh topology and refinement level around the fan and the fan tip gap.

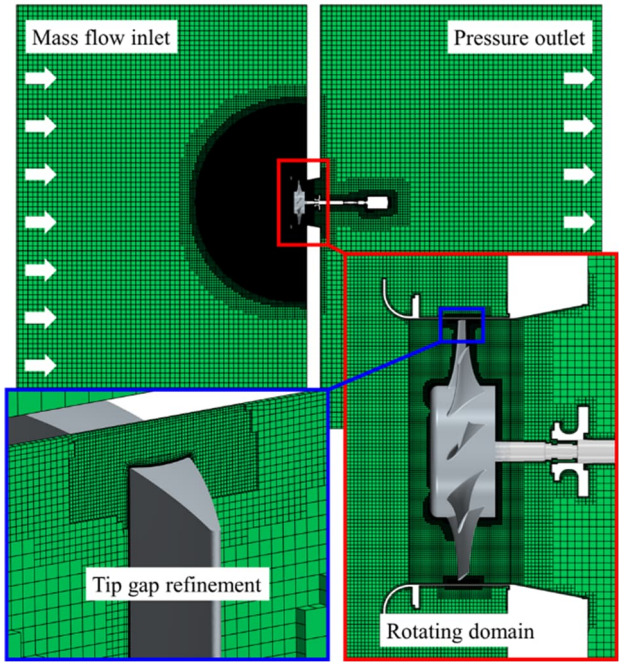

Figure 3. Finest volume mesh, topology and details.

All simulations were performed with Simcenter STAR-CCM+ version 2502. The unsteady, scale-resolving runs were initialized with a steady state Reynolds-averaged Navier-Stokes solution and utilize a segregated solver based on the SIMPLEC algorithm to solve the transient flow equations in an uncoupled manner. Fan motion was modelled with MRF for the steady, initial step and RBM for the unsteady part. The latter uses a wall-modelled Large Eddy Simulation (WMLES) approach based on the Wall-Adapting Local Eddy-Viscosity (WALE) subgrid-scale model [9] for turbulence modelling.
Each run featured eight fan revolutions with 2,000 time-steps per rotation, which equals 12.5 time-steps per period at 4 kHz. The convective wave equation is activated after the first rotation and the Newmark Alpha scheme uses $\alpha = -1/3$. Acoustics data sampling took place over the last six rotations.

4. RESULTS

In this section, we will analyze simulation results obtained on several operating points distributed over the entire characteristic fan curve. We will particularly investigate the dependency of these results on the spatial discretization on the fan blades, as well as the impact of the different motion modeling approaches. The key enabler for performing these numerous simulations were 8 NVIDIA A100 GPUs, each with 40 GB GPU memory. On this hardware, elapsed simulation times varied between 16.8 hours on Mesh 1 with RBM, and 6.8 hours on Mesh 3 with MRF, where MRF motion modeling accelerated the simulations by about 35% compared to RBM.

4.1 Analysis of different operating points

Typically, the degree of resolution of LES simulations of wall-bounded flows are judged upon the sizes of the dimensionless wall distance y^+, and the dimensionless cell sizes in the streamwise direction Δx^+, and the spanwise direction Δz^+ of the flow. These quantities are governed by

$$y^+ = \frac{u_\tau y}{\nu}, \Delta x^+ = \frac{u_\tau \Delta x}{\nu}, \text{and } \Delta z^+ = \frac{u_\tau \Delta z}{\nu}, \quad (3)$$

where u_τ is the friction velocity and ν the kinematic viscosity of the fluid, y is the wall distance of the cell center of the first cell next to the wall, and Δx and Δz denote the local edge lengths in the respective flow directions. Usual criteria [10] consider an LES simulation to be properly wall-resolved if

$$y^+ \sim 1, \Delta x^+ < 100, \text{and } \Delta z^+ < 30, \quad (4)$$

and wall-modeled if

$$y^+ > 30, \Delta x^+ \approx \Delta z^+ < 500. \quad (5)$$

In day-to-day engineering applications, the flow is usually not following a single, well-defined direction, and meshes are often isotropic on the wall. Hence, it is particularly difficult to judge the validity of the dimensionless cell sizes. In this paper, we approximate these quantities by evaluating

$$\Delta^+ := \frac{u_\tau \sqrt{A}}{\nu} \approx \Delta x^+ = \Delta z^+, \quad (6)$$

where A denotes the local face area at the walls.

The obtained upper limits for these values on the leading edges of the blades, and the blades themselves are presented in Table 2. It is evident that Mesh 1 can be considered a classical representative of a wall-resolved LES, whereas Mesh 4 is a clear representative of a wall-modeled LES, while Meshes 2 and 3 are hybrid states that independently vary y^+ or Δ^+.

Table 2. Realized wall discretization on the four considered volume meshes.

	Mesh 1	Mesh 2	Mesh 3	Mesh 4
Max. y^+ Leading Edge	1.2	4	6	14
Max. Δ^+ Leading Edge	22	14	26	50
Max. y^+ Blade	2.5	27	32	32
Max. Δ^+ Blade	98	85	166	320

In an initial attempt, the volumetric flow rate at the inlet was varied from 0.6 m³/s to 2.0 m³/s on the same grid and the mean total-to-static efficiency and total-to-static pressure coefficient were evaluated over the last sampled revolution of the fan. Figure 4 shows that especially the total-to-static pressure coefficient on Mesh 1 aligns very well with the test data.

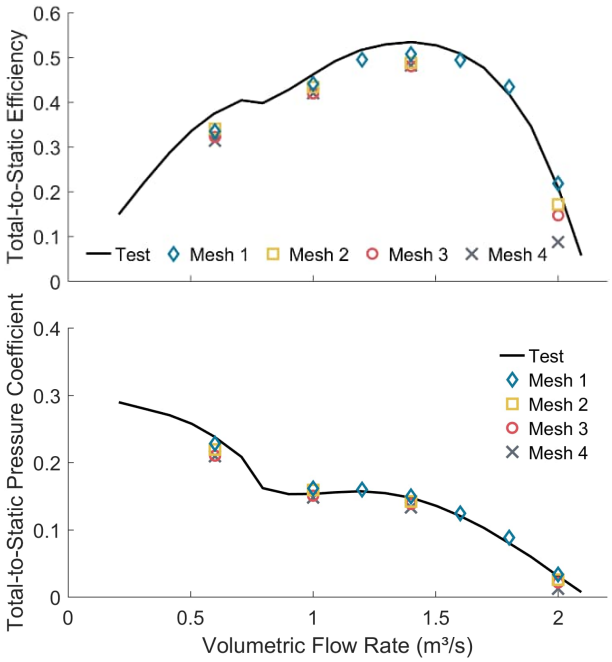

Figure 4. Mesh dependency of the total-to-static efficiency and pressure coefficient.

The efficiency shows slightly larger deviations, with a slightly flatter area around the design point and an underprediction at 0.6 m³/s. Based on these results, we decided to focus the further analysis on the limits of the expected fan operating range, 1.0 m³/s, and 2.0 m³/s, the design point 1.4 m³/s and the case at 0.6 m³/s. It is clearly visible that each individual mesh coarsening, including the independent increase of only y^+, leads to an increased under-prediction of the aerodynamic predictions. And even though this effect is most pronounced for the highest mass flow rate, the data points still follow the measured curves.

By inspecting the wall shear stress on Mesh 1 in Figure 5, one can identify the difference between the various volumetric flow rates: particularly at the lowest considered volumetric flow rate of 0.6 m³/s the flow is highly turbulent on the entire fan blade, and the vortical structures extend upstream throughout the whole shroud, typical for the stall regime. As the volumetric flow rate increases, the upstream vorticity drops, and the flow at the design point of 1.4 m³/s is dominated by the tip gap dynamics and becomes less turbulent on the blade.

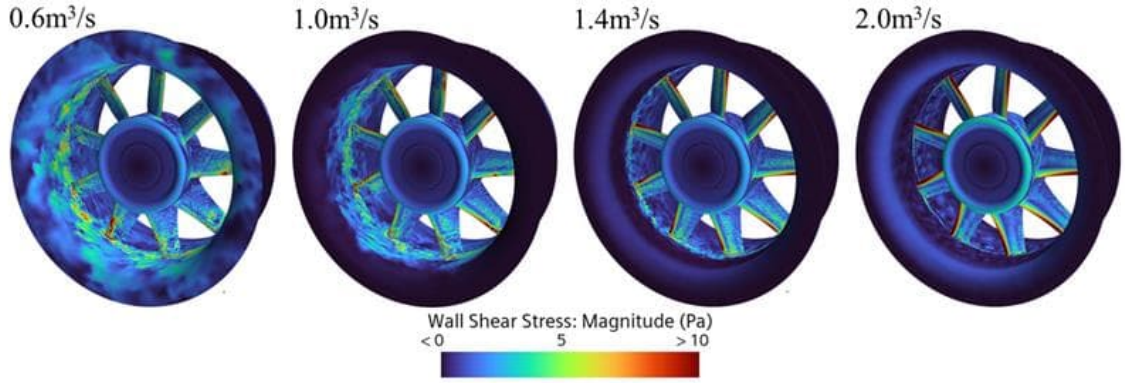

Figure 5. Instantaneous wall shear stress from Mesh 1 on fan and shroud.

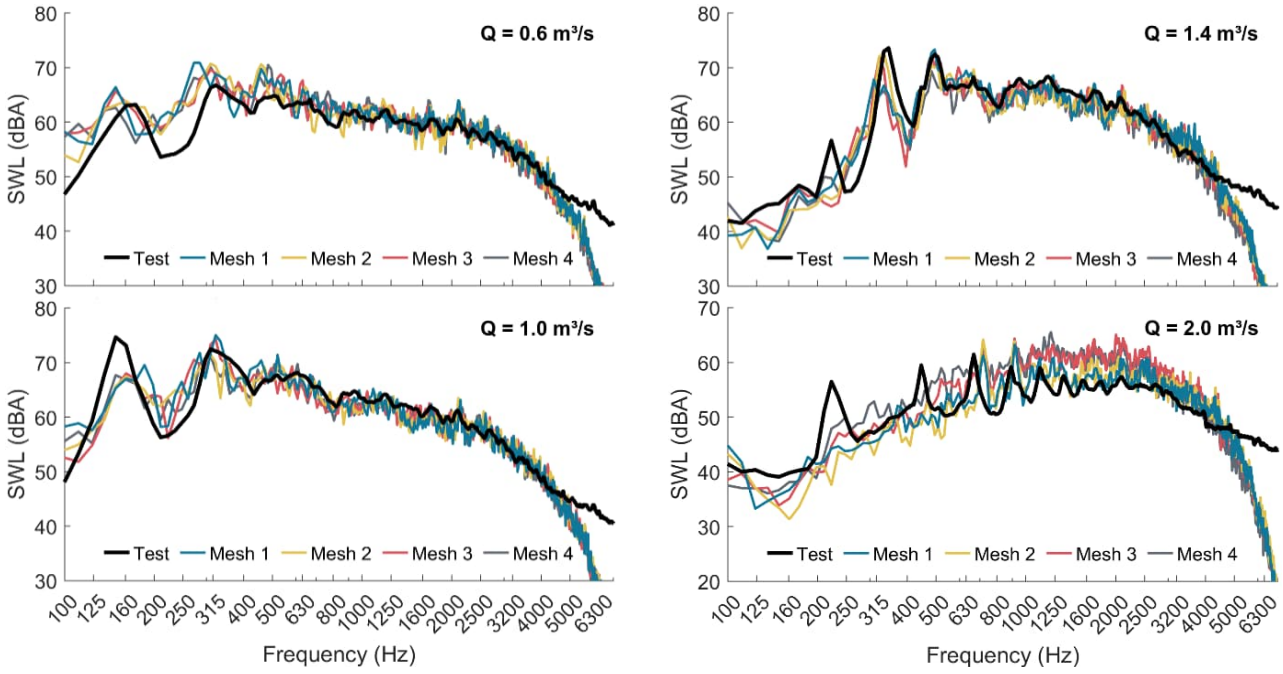

Figure 6. Mesh dependency of the Sound Power Level obtained from the 7 far field microphones.

Finally, at 2.0 m³/s, the trace of the tip gap vortex becomes much more localized and the flow around the blades transitions significantly later, a typical characterization of free flow conditions.

In this context, we can attempt to analyze the Sound Power measured at the 7 far field microphones which are shown in Figure 6. The test data from Krömer's experiments [8] shows a clear dependency on the considered operating point. The spectrum at the design point has already been analyzed in much detail [1, 8], and it is characterized by low low-frequency levels, which are followed by a relatively subtle peak at the blade passing frequency and two strong subharmonic peaks due to the tip gap dynamics. The highest frequencies above 2 kHz are then dominated by trailing edge noise of the blades. In comparison, the spectra at lower volumetric inflow rates show subharmonic peaks that are shifted to lower frequencies, and similar high frequency characteristics. In contrast, the spectrum at the highest volumetric inflow rate appears highly different: The subharmonic peaks vanish entirely, but the blade passing frequency with several harmonics is strongly excited. Furthermore, the overall level of the broadband high frequency content decreases by more than 5 dBA and finally remains more stable towards the highest frequencies.

The simulation results at the design point and the mass flow rate of 1.0 m³/s are highly consistent across all considered meshes and agree well with those reported in the literature, i.e. they show sensitivities at the subharmonic peaks, and they don't capture the blade passing tones. The results at the lowest volumetric inflow rate are also highly consistent and match excellently above 300 Hz, but they overpredict the noise due to the vortex dynamics at the lowest frequencies.

Overall, these results indicate that the acoustics predictions at these volumetric flow rates are much less sensitive to any meshing considerations than the aerodynamic quantities – which are presumably dominated by the strong tip gap vortex dynamics. In agreement with the aerodynamic results, the spectra at the highest volumetric inflow rate show the greatest dependency on the meshes: While the results from the finest mesh (Mesh 1) match the test results quite well, apart from the missing blade passing tones, the results on the coarsest grid leads to a strong offset of more than 5 dBA in almost the entire frequency range. However, it should be noted that the independent modification of y^+ does not affect the acoustic results, it is only the increase of Δ^+ that leads to deteriorated results. Hence, the aerodynamics seem to depend much more on the wall normal resolution in the vicinity of the wall, than the acoustics, which rely much more on the surface resolution. To understand the reasons for these differences, we can analyze the instantaneous wall shear stress and the surface trace of the acoustic source term of the PCWE in Figure 7. In these images, it is clearly visible that the flow structure around the blades changes immediately with increasing y^+, whereas the increase of Δ^+ in Mesh 3 and Mesh 4 only coarsens the flow pattern found on Mesh 2.

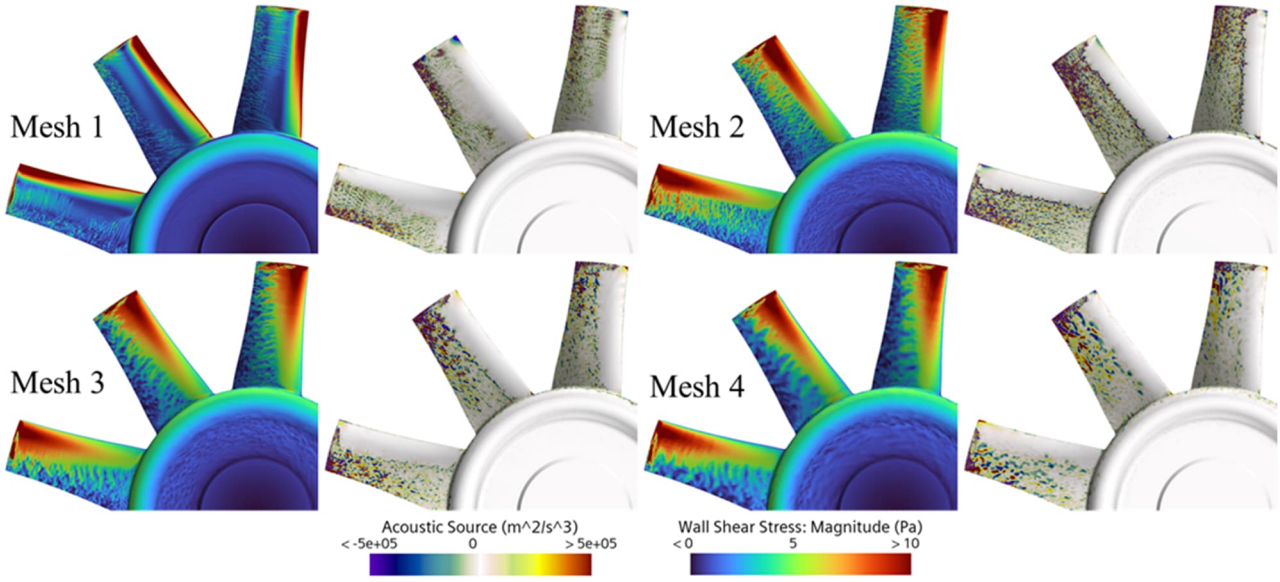

Figure 7. Wall shear stress and trace of the volumetric acoustic source term of the PCWE of the fan.

In contrast, it can also be seen that the acoustic source term changes going from Mesh 1 to Mesh 2, but we still see sources everywhere on the downstream parts of the blades. But with increasing Δ^+ on Mesh 3 and Mesh 4, the sources on the blade itself become weaker and the source term accumulates around the tip gap, which likely indicates a shift of the dominant noise generation mechanism.

4.2 Influence of Motion Modeling

Separately from coarsening the mesh or the time-step it is also possible to consider switching the motion modeling from RBM modeling with a rotating and a stationary domain, to MRF modeling that keeps a stationary mesh but introduces a moving reference frame. While this clearly reduces the computational costs per time-step, the individual impact on aerodynamics and acoustics predictions in a scale-resolving simulation is relatively unclear. To address this question, Meshes 1 and 3 were additionally simulated with MRF. In Figure 8, one can see the aerodynamics results on the different meshes and it can be clearly seen that the MRF motion modeling has a significant impact on both meshes, leading to bigger deviations from the test results. Again, particularly the volumetric inflow rate of 2.0 m³/s is most sensitive to these changes. Very much in contrast to this, especially the broadband acoustic results at the fan's design point shown in Figure 9 are consistent across the entire frequency range. Again, a big deviation is visible on Mesh 3 for the first subharmonic peak, which correlates well with strong sensitivity of the aerodynamic results on the motion modelling approach. The results on the other volumetric inflow rates were highly consistent with those from the design point.

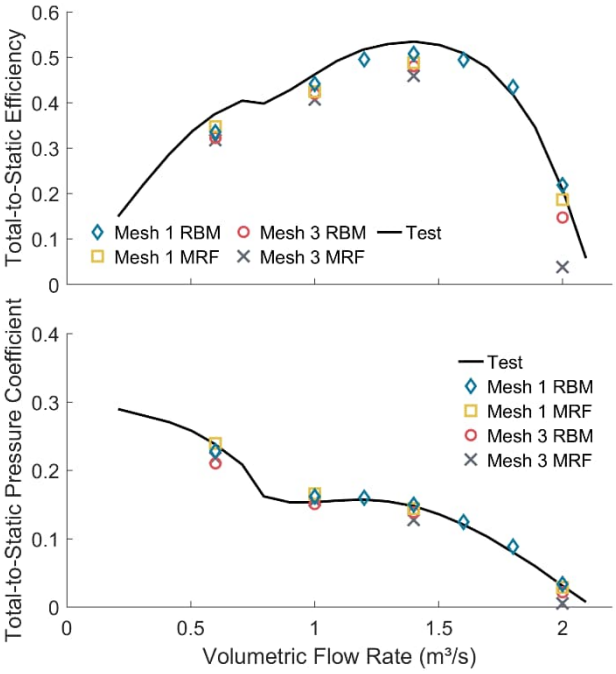

Figure 8. Dependency of the total-to-static efficiency and pressure coefficient on motion modeling.

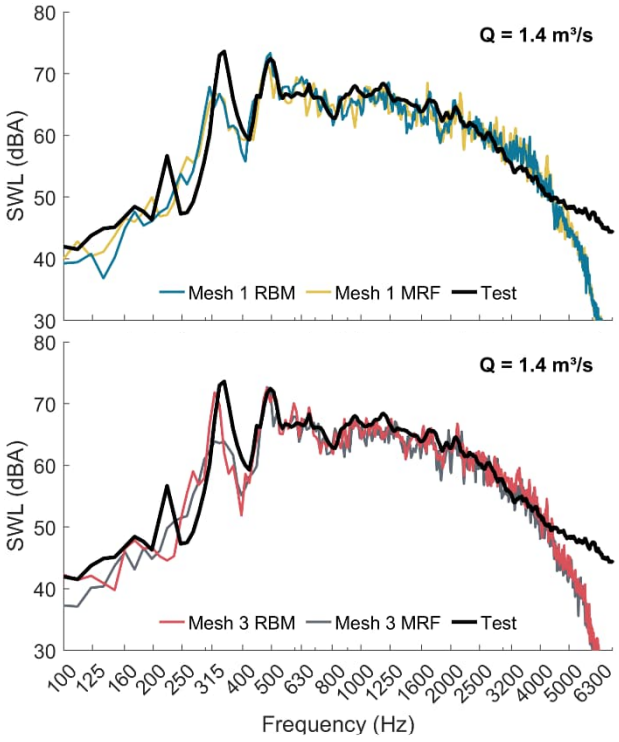

Figure 9. Dependency of the Sound Power Level obtained from the 7 far field microphones on motion modeling.

5. SUMMARY & CONCLUSION

In this paper, scale-resolving hybrid aeroacoustic simulations of the EAA benchmark fan across almost its entire operating range were performed on 8 NVIDIA A100 GPUs. The GPUs helped to reduce the computational costs of each simulation to significantly less than a day. In the simulations, we particularly studied the sensitivity of the aerodynamic and acoustic results on y^+ and Δ^+, as well as on different motion modelling approaches. The operating points were varied by modifying only the volumetric inflow rate. Overall, good results were achieved for all operating points without changing the mesh. It was found that the aerodynamic

predictions rely much more on highly resolved y^+ values and RBM than the acoustic results in the far field. Only the tones due to the subharmonic tip gap vortices as well as the free-flow operating point showed sensitivities to the Δ^+ mesh resolution and the motion modelling approach. Overall, this demonstrates that acoustics and aerodynamics converge at different rates towards their mesh-converged values.

Hence, one can potentially conduct comparably pragmatic acoustic simulations that do not attempt to answer aerodynamics and acoustics at the same time. Such an approach could be considered feasible in most of the fan's operating range. Such a split would be another step towards efficient utilization of the different length and timescales of aerodynamics and aeroacoustics.

To further investigate such splitting the authors intend to better understand the reasons for the mesh dependency at the free flow condition and look deeper into the vortex shedding mechanism at the blade tip. Furthermore, we intend to test these procedures on additional fan designs, such as those simulated by Ghodake [1] and further investigate the validity of MRF motion modelling in cases with more significant rotor stator interactions.

6. ACKNOWLEDGMENTS

The authors would like to thank Felix Czwielong and Stefan Becker from the Institute of Fluid Mechanics of Friedrich-Alexander Universität Erlangen-Nürnberg for providing the additional test data and for consenting to this publication.

7. REFERENCES

[1] Ghodake, D., et al.: "Effect of Sweep on Axial Fan Noise Sources Using the Lattice Boltzmann Method," in *Int. J. of Turbomachinery, Propulsion and Power*, vol. 7, no. 4, 2022.

[2] Antoniou, E., et al.: "Numerical flow noise simulation of an axial fan with a Lattice-Boltzmann solver," in *Acta Acustica*, 7, 65, pp. 1–14, 2023.

[3] L. Erbig, and S. Lardeau: "Hybrid Aeroacoustic Simulation of EAA's Axial Fan Benchmark," in *Fortschritte der Akustik – DAGA 2022*, (Stuttgart, Germany), pp. 360–363, 2022.

[4] EAA benchmark database, URL: https://eaa-bench.mec.tuwien.ac.at/

[5] Piepiorka, J. and Estorff, O.: "Numerical investigation of hydrodynamic/acoustic splitting methods in finite volumes including rotating domains," in *Proc. of the 23rd Int. Congress on Acoustics*, (Aachen, Germany), 2019.

[6] Siemens Industry Software, Simcenter STAR-CCM+ User Guide, Version 2502, 2025

[7] S. Schoder, C. Junger, and M. Kaltenbacher: "Computational aeroacoustics of the EAA benchmark case of an axial fan," in *Acta Acustica*, 4, 22, pp. 1–17, 2020.

[8] Krömer, F: "Sound emission of low-pressure axial fans under distorted inflow conditions," Erlangen: FAU University Press, 2018.

[9] Nicoud, F. and Ducros, F.: "Subgrid-Scale Stress Modelling Based on the Square of the Velocity Gradient Tensor," in *Flow, Turbulence, and Combustion*, vol. 62, no. 3, pp. 183–200, 1999

[10] J. Fröhlich: *Large Eddy Simulation turbulenter Strömungen*. Wiesbaden: Vieweg+Teubner Verlag, 2007.